Near-optimal Velocity Control for Mobile Charging in Wireless Rechargeable Sensor Networks

Yuanchao Shu, *Member, IEEE,* Hamed Yousefi, *Student Member, IEEE,* Peng Cheng, *Member, IEEE,* Jiming Chen, *Senior Member, IEEE,* Yu Gu, *Member, IEEE,* Tian He, *Senior Member, IEEE,* and Kang G. Shin, *Life Fellow, IEEE*

Abstract—Limited energy in each node is the major design constraint in wireless sensor networks (WSNs). To overcome this limit, wireless rechargeable sensor networks (WRSNs) have been proposed and studied extensively over the last few years. In a typical WRSN, batteries in sensor nodes can be replenished by a mobile charger that periodically travels along a certain trajectory in the sensing area. To maximize the charged energy in sensor nodes, one fundamental question is how to control the traveling velocity of the charger. In this paper, we first identify the optimal velocity control as a key design objective of mobile wireless charging in WRSNs. We then formulate the optimal charger velocity control problem on arbitrarily-shaped irregular trajectories in a 2D space. The problem is proved to be NP-hard, and hence a heuristic solution with a provable upper bound is developed using novel spatial and temporal discretization. We also derive the optimal velocity control for moving the charger along a linear (1D) trajectory commonly seen in many WSN applications. Extensive simulations show that the network lifetime can be extended by $2.5\times$ with the proposed velocity control mechanisms.

Index Terms—Wireless rechargeable sensor networks, velocity control, energy harvesting, mobile charging

1 Introduction

Limited energy at each node in wireless sensor networks (WSNs) is known to be the major hurdle in their design and operation [1]–[5]. Wireless energy transfer technology, enabling the transmission of electrical energy from a charger to sensor nodes, paves a new way of replenishing the energy or extending the lifetime of sensor nodes. This technology is exploited by wireless rechargeable sensor networks (WRSNs) which have been drawing significant interests from the WSN research community.

As one type of wireless power transfer (WPT) systems, architects of WRSNs face a couple of choices in the energy transfer technique, among which the (non-radiative) magnetic induction and the electromagnetic radiation harvesting are most commonly discussed.

Inductive power transfer works by creating an alternating magnetic field (flux) in a transmitter coil and converting that flux into an electrical current in the receiver coil [6]. The transmit and receive coils are tightly coupled when (a) the coils have the same size, and (b) the distance between the coils is much less than the diameter of the coils. Though bringing less losses, a higher coupling factor trades-off higher power transfer efficiency at the cost of smaller distance and limited flexibility. From the beginning of inductive power transmission, resonant circuits have been used to enhance the efficiency of power transmission. For example, Nikola Tesla used resonance techniques in his first experiments with inductive power transmission in 1891. However, as resonance cannot be achieved simultaneously at two tightly coupled coils, either tightly coupled coils or the resonant coupling technique is adopted by current WPT manufacturers. For example, Qi transmitters use tight coupling between coils, and operates the transmitter at a frequency that is slightly different from the resonance frequency of the receiver [7].

In addition to inductive power transfer, radio frequency (RF) energy is another form best suited to energy transfer. RF energy is currently broadcasted from billions of radio transmitters around the world, including mobile telephones, handheld radios, RFID readers, mobile base stations, and television/radio broadcast stations. Battery-based systems can be trickled charged to eliminate battery replacement or extend the operating life of systems using disposable batteries [8]. Battery-free devices can also be designed to operate on demand or when sufficient charge is accumulated [9]. In both cases, these devices can be free of connectors, cables, and battery access panels, and have freedom of placement and mobility during charging and usage.

The wireless charging technologies, listed in Table 1 below, differ in the type of oscillating electromagnetic field, the distance over which they can transmit power, the energy conversion effi-

- *Y. Shu is with Microsoft Research Asia, Beijing, China. Email: yushu@microsoft.com*
- *P. Cheng and J. Chen are with the State Key Lab. of Industrial Control Technology, Zhejiang University, Hangzhou, China. Email: {pcheng, jmchen}@iipc.zju.edu.cn*
- *H. Yousefi is with Department of Computer Engineering, Sharif University of Technology, Tehran, Iran. Email: hyousefi@ce.sharif.edu*
- *Y. Gu is with IBM Watson Health, Austin, TX, USA. Email: yugu@us.ibm.com*
- *T. He is with Department of Computer Science and Engineering, University of Minnesota, MN, USA. Email: tianhe@cs.umn.edu*
- *K. G. Shin is with Department of Electrical Engineering and Computer Science, The University of Michigan, Ann Arbor, MI, USA. Email: kgshin@umich.edu*

Manuscript received January 15, 2015; revised May 24, 2015, August 2, 2015; accepted August 13, 2015.

Table 1
Comparison of different wireless charging techniques

Charging Technology	EM Field	Distance	Efficiency	Freedom	Consortia (standard)	Example Product (consortia)
Magnetic resonance	Near field	Medium	High	Medium	A4WP (Rezence), WPC (Qi extension)	WiPower (A4WP), PowerbyProxi (Qi)
Magnetic induction		Short	Medium	Low	PMA, WPC (Qi)	Powermat (PMA), PowerbyProxi (Qi)
RF energy harvesting	Far field	Far	Low	High	–	WISP, Moo, Powercast, WattUp (PMA)

ciency, freedom of receiver during the charging process, and the consortia (or standard) they belong to. Three wireless charging technologies have their own advantages and drawbacks. For example, resonant inductive coupling achieves the highest charging efficiency by using resonant circuits whereas far field methods achieve longer ranges (even multiple kilometers [10]). As with any technology, there are a number of systems looking to gain dominance and become "the standard" of wireless charging. As is currently stands, there are three consortia each promoting their vision for the de-facto future standard of wireless charging: the Wireless Power Consortium (WPC), Alliance for Wireless Power (A4WP), and Power Matters Alliance (PMA)[1].

Given the advantages of WPT, a WRSN is a promising platform for various applications, including warehouse inventory management [12], [13], large-scale urban sensing [14], access authentication [15], and structural health monitoring [16]. In these applications, mobile chargers are good candidates for charging WRSN nodes [17]–[19]. Compared to deploying multiple static wireless chargers, using one mobile charger is cost-efficient and flexible in dealing with network topology changes. Moreover, the mobile charger can be combined with the mobile base station to help alleviate network congestion and avoid energy hot spots during data collection. In most mobile charging scenarios, the movement of the charger is time- and space-constrained. For example, in warehouse, environmental and structure monitoring applications, chargers carried by vehicles/robots are only able to travel along fixed trajectories [20], [21]. In mission-critical applications, if a time-shared charger is used to charge distributed clusters of sensor nodes, it has to finish each charging job and reach a neighboring area within a certain time limit to charge energy-deficient nodes there. In inventory control/port management systems where a charger is co-located with a mobile base station to gather time-sensitive data, there exist strict timing constraints on both charging and data gathering [22]–[24]. Furthermore, a time-bounded tour guarantees that the charger be replenished at the start point (or the home service station) in a timely manner [24].

However, mobile charging creates several challenges in energy provision in WRSNs. One fundamental challenge is how to control the speed of the mobile charger. In the case of omnidirectional wireless charging, the amount of energy charged in nodes is dictated by 1) the distance between sensor nodes and the charger, and 2) the duration of charging each node. Specifically, the charging power at nodes decreases as the distance to the charger increases. Given a fixed charging distance, the charged energy at nodes increases with the charging duration. It is thus desirable to charge nodes as long as possible and at minimum distances from the charger. However, due to location diversity, the charged energy at different nodes cannot be maximized simultaneously. If we choose to fully charge part of the network, there may not be enough time for the charger to move and charge other parts of the network, especially under the time-bounded charging constraint. Thus, given constrained moving trajectories, the velocity of the charger plays an important role in energy provision in WRSNs. Due to the non-uniform distribution of sensor nodes and different shapes of the moving trajectory, it is non-trivial to continuously determine if the charger should move faster or slower along the trajectory, in order to maximize the charged energy at nodes.

In this paper, we consider a common scenario where the charger travels along a pre-planned trajectory and determine the optimal velocity of the charger subject to a given traveling time constraint, such that the network lifetime is maximized. Specifically, we aim to maximize the minimum charged energy among all nodes in the network. This way, we can mitigate the uneven energy replenishment of sensor nodes which has a significant effect on sensing quality, data delivery reliability, network throughput, and so on [25]. This paper makes the following three main contributions.

- To the best of our knowledge, this is the first attempt to identify the velocity control of a mobile charger for the time-bounded charging scenario with a fixed trajectory in WRSNs. Using both theoretical analysis and extensive simulations, we demonstrate the advantages of the proposed velocity control.
- We analyze the velocity control problem in a general 2D space where the charger is moving along an arbitrarily-shaped trajectory. As a first step, we narrow the problem scope to a manageable single-node charging scenario and then extend it to the multiple-node scenario. After proving the NP-hardness of the problem, we propose a heuristic solution with a provable upper bound using novel spatial and temporal discretization.
- Considering the prevalent use of straightline moving trajectories in many applications, such as pipeline and bridge monitoring [26], [27] and coal mine tunnel monitoring [28]), we also propose the optimal velocity control mechanism for a linear trajectory.

The rest of the paper is organized as follows. Section 2 discusses related work. Section 3 provides the system model and the problem formulation. Section 4 describes our velocity control mechanism for the general 2D trajectory. Section 5 covers a special case where the charger is moving along a linear trajectory. Section 6 evaluates the performance of the proposed solutions while Section 7 discusses several related practical issues. Finally, Section 8 concludes the paper.

2 Related Work

Recently there has been a surge of interest in the field of WRSNs, where a single mobile charger travels through the network to replenish energy to sensor nodes through strongly-coupled magnetic

1. The latter two consortia, A4WP and PMA, have agreed to merge in early 2015 to help promote their standards (e.g., Rezence) as an alternative to the more established Qi standard proposed by WPC [11].

resonances [29] or radio frequency (RF) signals [9], [30]. Peng *et al.* [31] studied the feasibility of using the wireless charging technology to prolong the sensor network lifetime in a prototype system. Shi *et al.* [32] investigated the problem of periodically charging sensors inside the network to maximize the ratio of charger's vacation time over a cycle. They extended the problem to the case where multiple nodes can be charged at the same time [33], [34]. Fu *et al.* [19] planned an optimal movement strategy of the charger, such that the time to charge all node's onboard energy storages above a threshold is minimized. The tradeoff between the number of sensors that an energy-constrained charger can charge and the distance it can move was studied in [35]. In [36], Angelopoulos *et al.* proposed distributed and adaptive protocols that use limited network information to address three key issues: (1) to what extent each node should be charged, (2) what is the best split of the total energy between the charger and sensor nodes, and (3) what are good trajectories the mobile charger should follow. The impact of mobility on energy provisioning in WRSNs based on node spatial distributions was studied in [37]. He *et al.* [1] proposed an empirical recharge model based on experimental data and studied the energy provisioning problem to decide on the deployment of charges to guarantee perpetual operation of the source nodes in a WRSN. Cheng *et al.* [38] investigated the problem of jointly mobilizing the charger and scheduling sensor nodes for efficient charging distribution and optimal event capture.

There also some studies on taking advantage of the network capability to support more than one mobile charger. In [17], collaboration among multiple vehicles to recharge not only the sensor nodes but also each other vehicles in a 1D network was studied so that a larger network can be covered. Wang *et al.* [39] studied how to minimize the total traveling cost of multiple chargers while ensuring no node failure. Dai *et al.* [40] investigated the minimum number of energy-constrained mobile chargers and their recharging routes in a 2D WSN, so as to keep the network running forever. Madhja *et al.* [41] addressed two main issues: what are good coordination procedures for the mobile chargers and what are good trajectories for the mobile chargers, and proposed new central and distributed protocols for efficient recharging.

In [42], [43], the authors proposed efficient schemes in which the routing and charging procedures are performed jointly. Moreover, in [18], [22]–[24], a mobile charger is used to serve not only as an energy transmitter to charge static sensor nodes, but also as a data collector to maximize the network lifetime.

In spite of a rich heritage of work in WRSNs, there is no study on the optimal velocity control for efficiently charging the sensor nodes. This paper has investigated this new problem for the first time to the best of our knowledge.

3 System Model and Problem Formulation

We first introduce the system model of a WRSN and then formulate the problem of controlling a mobile charger's velocity.

3.1 System Model

The network under consideration consists of N rechargeable sensor nodes deployed in a 2D area Ω with each node i's position p_i known. (Note that after deploying sensor nodes, p_i can be determined by using various localization methods, such as [44].)

An example of charging a WSN with one mobile charger is depicted in Figure 1, where the charger moves periodically along trajectory D in Ω while charging the sensor nodes in its vicinity.

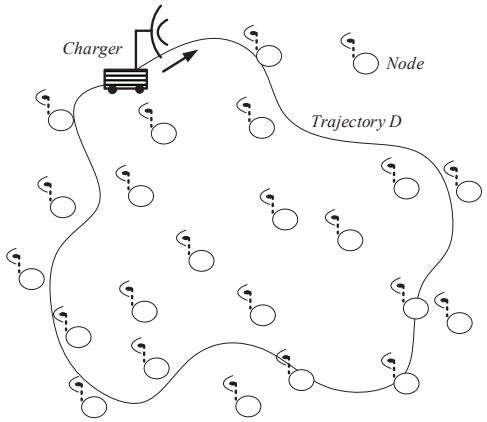

Figure 1. An example charging scenario

The traveling time of the charger's single trip is defined as the *patrolling cycle* T, which is given as a timing constraint. Let $v(t)$ and $a(t)$ denote, respectively, the charger's velocity and acceleration at time t within each T. We also assume that the charger is equipped with a battery with enough capacity to broadcast a radio signal at maximum transmission power during an entire trip.

We assume an omnidirectional wireless charging model in which the wireless charging power at different nodes is dictated by two factors: 1) the distance between nodes and the charger, and 2) the transmission power of the charger. Specifically, we adopt the following empirical wireless charging model based on our previous experimental results [1]:

$$P_{rx}(d) = \frac{\tau}{(d+\beta)^2}, \tag{1}$$

where $\tau = \frac{G_{tx}G_{rx}\eta}{L_p}(\frac{\lambda}{4\pi})^2 P_{tx}$ is a known constant determined by the hardware of the charger and receivers (sensor nodes). P_{tx} is the source power, G_{tx} is the source antenna gain, G_{rx} is the receiver antenna gain, λ is the wavelength, L_p is the polarization loss, η can be referred to as the rectifier efficiency, and d is the physical distance between the charger and a rechargeable receiver. From our extensive experimental tests, we obtained the parameter $\beta = 0.2316$ after applying the least square technique for fitting the experimental data [1].

3.2 Problem Formulation

Our goal is to maximize the network lifetime during each patrolling cycle T by controlling the charger's velocity.

The problem can be stated formally as:

$$\textbf{maximize} \quad \min_i(\int_0^T P_i(t)dt - \gamma_i T) \tag{2}$$

$$s.t. \quad P_i(t) = P_{rx}(d_i(t)),\ i \in \{1,\ldots,n\} \tag{3}$$

$$\int_0^T v(t)dt = L \tag{4}$$

$$|a(t)| \le \alpha, \tag{5}$$

where $\int_0^T P_i(t)dt$ in (2) is the harvested/recharged energy at node i and $\gamma_i T$ is the amount of its energy depleted during T. The constant depletion-rate γ_i can be obtained from the network settings, such as the sensors' operation schedule and transmission mode [32], [45]. For example, the sensors close to the sink node in a monitoring system will consume energy at high rates, thus resulting in larger γ values. To maximize the network lifetime, we

focus on maximization of the term $\int_0^T P_i(t)dt$ for the node i with the least amount of energy during T.

We call the corresponding charger's velocity, $v(t)$, of (2) the *optimal velocity profile* R^*. Different velocity profiles of the charger correspond to different velocity–time curves from $t = 0$ to $t = T$. Eq. (3) characterizes the relationship between charging power at node i and its distance from the charger. Eq. (4) guarantees the patrolling requirement of the charger. Inequality (5) represents the acceleration constraint where α is the charger's maximum acceleration/deceleration.[2] The symbols and notations used in this paper are summarized in Table 2.

Table 2
Notation definition

Symbol	Meaning
N	Number of nodes
p_i	Position of node i
$v(t)$	Traveling velocity of the charger at time t
$a(t)$	Acceleration of the charger at time t
α	Maximum value of acceleration of the charger
T	Patrolling cycle of the charger
D	Trajectory
L	Length of trajectory
$P_i(t)$	Charging power at node i at time t
E_i	Total charged energy of node i
γ_i	Energy depletion rate of node i

Note that to maximize network lifetime, we simplify the problem and maximize the charged energy of the node with the minimum harvested energy in the network. However, our model can be easily extended to maximize the energy balance of the M-th node when nodes are sorted in ascending order of their charged energy (see Section 7).

4 Design

We now address how to control the velocity of a charger that moves along an arbitrarily-shaped pre-defined trajectory in a 2D space. The non-linear continuous changes of $d_i(t)$ make the objective function (2) non-convex, thereby making the conventional convex optimization inapplicable. Moreover, the velocity-control space is infinite, so it is difficult to realize continuous velocity control. We tackle these issues by introducing a novel discretization method that solves the velocity control problem by effectively making a tradeoff between computation accuracy and overhead. As a first step and to further illustrate the problem, we start with the single-node case and propose a solution with a provable degree of suboptimality. We then extend the solution to the multi-node case with performance bounds.

4.1 Single Node with an Arbitrary 2D Trajectory

We discretize the velocity control in both temporal and spatial dimensions.

4.1.1 Temporal Discretization

In a generic mobile charging scenario, the charger is mounted on a vehicle or a robot which may change its velocity. Considering the limited acceleration capability of a robot/vehicle, we discretize the charger's velocity. In contrast to the continuous velocity model (Figure 2(a)), we present a discrete velocity model in which the charger's velocity can change only at discrete time $t = m\Delta t,\ m \in \mathbb{N}$, and hence remains constant between two adjacent discrete time instants (Figure 2(b)). *Time slot* Δt is the minimum duration between two adjacent velocity changes and $T = n\Delta t$. In other words, $\frac{1}{\Delta t}$ is the maximum frequency of the charger's velocity changes. The hold time of each velocity value is called the *period*, which is an integer multiple of Δt. Since the charger's acceleration is less than α, the velocity difference between two consecutive periods is bounded by the period length. Therefore, from (5), we have

$$|v_i - v_{i-1}| \leq \alpha t_i, \tag{6}$$

where v_i is the velocity at the i-th period and t_i is the length of this period.

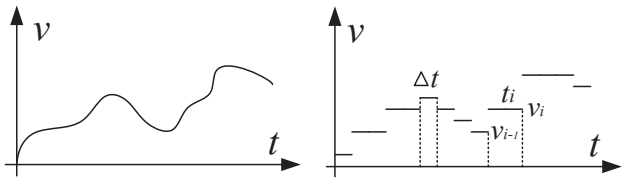

(a) Continuous velocity (b) Discrete velocity

Figure 2. Velocity discretization

4.1.2 Spatial discretization

In addition to the temporal discretization, we discretize the arbitrary trajectory spatially based on the charging power. To this end, we first determine the nearest and farthest points on the trajectory which have the highest and lowest charging power at the charging node q. Let $P_q^{\max}$ and $P_q^{\min}$ be the charging power at node q of these two points on the trajectory. To discretize the charging power at node q, we draw C_q concentric circles around q with an increasing radius. Specifically, given a small enough discretization factor ϵ ($\epsilon > 0$), the charging power between neighboring circles can be represented by a vector of discretized charging powers as $P_q = [P_q^1, P_q^2, \ldots, P_q^{C_q}]$, where

$$P_q^g = P_q^{\max}(1+\epsilon)^{-g},\ 1 \leq g \leq C_q. \tag{7}$$

In 7, C_q can be calculated as $C_q = \left\lceil \frac{\ln \frac{P_q^{\max}}{P_q^{\min}}}{\ln(1+\epsilon)} \right\rceil$. This way, we divide the original irregular trajectory D into k segments with respect to the charging power at node q. The difference of charging power between neighboring segments (as well as circles) is bounded by the threshold ϵ. Instead of calculating the charging power at different positions on the trajectory, we use the lower bound of the charging power of each segment, i.e., the charging power at positions on different circles.

Taking Figure 3(b) as an example, trajectory D is divided into six segments ($D_1, \ldots, D_6$ where $k = 6$) within three ($C_i = 3$) regions, i.e., region S_1 (red), S_2 (blue) and S_3 (green). Charging powers at different positions on D_1 are identical and equal to $P_q^{\max}(1+\epsilon)^{-1}$. Similarly, charging powers at different positions on D_2, D_4 and D_6 are equal to $P_q^{\max}(1+\epsilon)^{-2}$, and charging powers on D_3 and D_5 are $P_q^{\max}(1+\epsilon)^{-3}$.

2. We consider the same bound for both acceleration and deceleration. But our algorithm can be extended to more realistic cases where bounds of acceleration and deceleration are different. This extension will be discussed in Section 7.3.

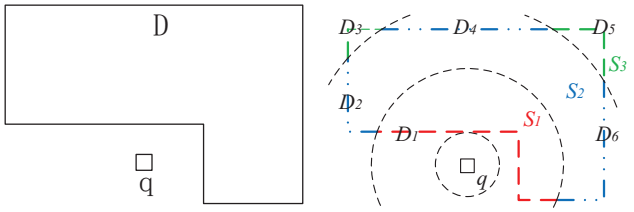

(a) Before discretization (b) After discretization

Figure 3. Trajectory discretization

4.1.3 Velocity control

Based on the discrete velocity and discretized trajectory, we design a velocity control mechanism by assigning the patrolling cycle T to different segments of the trajectory. Specifically, for the single node case, the velocity control problem can be stated as:

$$\textbf{maximize} \quad \sum_{j=1}^{k} p_1^j t_j \tag{8}$$

$$s.t. \quad \sum t_j = T \tag{9}$$

$$|\tfrac{L_j}{t_j} - \tfrac{L_{j-1}}{t_{j-1}}| \leq \alpha t_j, \ \forall j \in [2,k] \tag{10}$$

$$\tfrac{L_j}{t_j} \leq \alpha t_j, \ j \in \{1,k\} \tag{11}$$

where period $t_j = m\Delta t, \ m \in \mathbb{N}$ is the traveling time of the charger on the j-th segment and L_j is the length of the j-th segment of the trajectory. Eqs. (8) corresponds to Eqs. (2) which denotes the charged energy. Due to the unique approximated charging power of each segment, the harvested energy at nodes is only related to the charger's traveling time, and hence the charger moves at a constant velocity $\frac{L_j}{t_j}$ within the j-th segment. Eqs. (9) refers to the bound of traveling time. Eqs. (10) and (11) are derived from (6) to satisfy the acceleration requirement α in Section 3.2. The physical meaning of the above assignment problem can be described as: **Given the patrolling cycle T which is temporally discretized into n time slots, assign all n slots to the k segments of the trajectory in order to maximize the charged energy at the node.**

We first find the optimal substructure of this problem and then solve it by dynamic programming.

Given n candidate time slots and k segments, let $A(n,k)$ be the charged energy at node q with the optimal traveling time assignment. Then, we have the following optimal substructure in the traveling time assignment problem:

$$A(n,k) = \max_{i=1}^{n-k+1} [A(n-i,k-1) + E(i,k)] \tag{12}$$

where $E(i,k)$ is the charged energy of node q if the charger travels on the k-th segment for i slots. Assuming $n \gg k$, we have $1 \leq i \leq n-k+1$ because at least one time slot needs to be assigned to a segment.

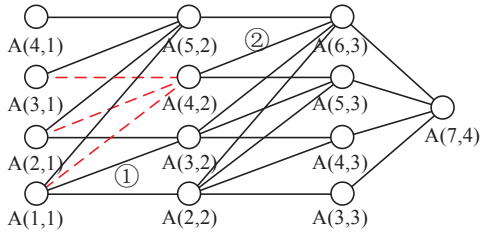

Figure 4. Optimal substructure graph

We use a graph to represent the optimal substructure of the traveling time assignment problem. Figure 4 shows an example of assigning 7 slots to 4 segments. Edges in this figure represent $E(i,k)$, e.g., edge ① refers to $E(2,2)$. The connection between A(1, 1) and A(3, 2) means that if we assign the first slot to the first segment (i.e., A(1, 1)) and the following two slots to the second segment (i.e., E(2, 2)), in total we assign the first three time slots to the first two segments (i.e., A(3, 2)).

With the optimal substructure, we adopt dynamic programming to solve the traveling time assignment problem. The main idea of generating the optimal substructure graph G is described in Algorithm 1. We first initialize G with $(k-1)$ columns and $(n-k+1)$ vertices in each column. Lines 3-5 initialize values of vertices in the first column, i.e., calculate charged energy $A(i,1)$ as the initial conditions of dynamic programming.

Algorithm 1 *Velocity Control Algorithm with a Single Node*

```
1: Input: L, T, α, ϵ, n, k, P_q
2: Init graph G
3: for each i ∈ [1, n − k + 1] do
4:     Calculate A(i, 1)
5: end for
6: for each j ∈ [1, k − 2] do
7:     for each i ∈ [j, j + n − k] do
8:         for each s ∈ [i + 1, j + n − k + 1] do
9:             Calculate E(s − i, j + 1)
10:            for each r ∈ [1, i − 1] do
11:                if 10 and 11 is true then
12:                    Connect A(i, j) and A(s, j + 1)
13:                    Update A(s, j+1)_i = max(A(s, j+1)_i, A(i, j)_r +
                       E(s − i, j + 1));
14:                end if
15:            end for
16:        end for
17:    end for
18: end for
19: for each i ∈ [n − k, n − 1] do
20:    if 10 and 11 is true then
21:        Connect A(i, k − 1) and A(n, k)
22:        Calculate E(n − i, k)
23:        Update A(n, k);
24:    end if
25: end for
26: return A(n, k)
```

Then, for each vertex in different columns, we decide whether it should be connected with nodes in its neighboring column based on the acceleration constraints (10) and (11). If it is true, we update the value of node in the right column. Note that due to (10) and (11), the value of each vertex in the right column depends on both its parent nodes and the parent nodes of its parent nodes. For instance, to update the value of $A(4,1)$, we need to consider one of its parent nodes, $A(3,1)$. However, the edge between $A(4,1)$ and $A(3,1)$ is related to three inbound edges of vertex $A(3,1)$ (red dashed edges in Figure 4) due to the acceleration constraint. Therefore, unlike the classic shortest path problem, the value of each vertex $A(i,j)$ in Algorithm 1 is a tuple which stores the values of paths from all its i parent nodes. For example, $A(3,1)$ is a 3-tuple and $A(4,1)$ updates itself based on the minimum value of $A(3,1)$ while satisfying (10) and (11).

Finally, we connect vertices of the last column and $A(n,k)$, and update its value at the same time (lines 17-23). The return value of $A(n,k)$ means the maximized charged energy of the node and we can trace back to find the corresponding optimal velocity

profile of the charger. It is easy to prove that the computation complexity of Algorithm 1 is $O(n^4)$.

4.1.4 Suboptimality

We now prove the suboptimality of the proposed velocity control algorithm. The suboptimality is defined as the ratio of actual amount to the optimal amount of charged energy.

Let E^* be the corresponding maximal charged energy of node q with the *optimal velocity profile* R^*, all of which are unknown. Then, we have the following theorem.

Theorem 4.1. *Given the velocity profile R_s derived from Algorithm 1 with its corresponding charged energy at node q E_s and $\epsilon > 0$, we have $E^* \leq E_s(1+\epsilon)$.*

Proof. Given ϵ, we can cut D into a unique set of segments. Let $\mathbf{t}^* \in \mathbb{R}^{k\times 1}$ and $\mathbf{t}_s \in \mathbb{R}^{k\times 1}$ denote the corresponding traveling durations of the charger in each segment under velocity profiles R^* and R_s, respectively. Specifically, $\mathbf{t}^*$ and $\mathbf{t}_s$ are two k-dimensional vectors with each element representing the traveling time on each of these k segments. Let $\mathbf{P}_q^* \in \mathbb{R}^{1\times k}$ denote the average actual charging power of segments under the optimal velocity profiles R^*. That is, $E^* = \mathbf{P}_q^*\mathbf{t}^*$ and both of $\mathbf{P}_q^*$ and $\mathbf{t}^*$ are unknown. Similarly, $\mathbf{P}_q \in \mathbb{R}^{1\times k}$ is denoted as the approximated charging power vector under the velocity profiles R_s.

Since Algorithm 1 provides the optimal traveling duration on each segment under the scenario with discretized charging power $\mathbf{P}_q$, we have

$$E_s = \mathbf{P}_q\mathbf{t}_s \geq \mathbf{P}_q\mathbf{t}^*. \tag{13}$$

Unlike E_s, E^* can hardly be represented as R^* is an unknown continuous function. However, since the charging power at any position in region S_j is always smaller than $P(S_{j-1})$ through spatial discretization, $\mathbf{P}_q^*$ is bounded by $\mathbf{P}_q(1+\epsilon)$ in each segment. Therefore combining with (13), we have

$$E_s = \mathbf{P}_q\mathbf{t}_s \geq \mathbf{P}_q\mathbf{t}^* \geq \mathbf{P}_q^*/(1+\epsilon)\mathbf{t}^* \geq E^*/(1+\epsilon). \tag{14}$$

Hence, for any ϵ, $E^* \leq E_s(1+\epsilon)$. The proof is complete. □

4.2 Multiple Nodes with an Arbitrary 2D Trajectory

We now extend the proposed velocity control mechanism to a general case where the charger moves along an irregular trajectory to charge multiple nodes. As stated in Section 3.2, we want to maximize the energy budget of the "bottleneck" node — the node which has the least amount of charged energy — in order to extend the network lifetime. We first prove the problem is NP-hard and then propose a heuristic algorithm with performance bounds.

4.2.1 Proof of NP-hardness

We reduce a known NP-hard problem, the Multi-Objective Shortest Path problem (MOSP) [46], [47], to our velocity control problem to prove its NP-hardness.

Definition of Multi-Objective Shortest Path Problem: Given a directed graph $G = (V, A)$, with $V = \{1, \ldots, n\}$ and $|A| = m$, and a set S of k scenarios for each arc $(i, j) \in A$ and its cost c_{ij}^s, $s \in S$, MOSP aims to find the shortest path of G which has the minimal Σc.

In MOSP, the objective function is formulated as a linear function or max-min (or min-max) function. These two objectives correspond to the "sum" problem and the "bottleneck" problem, respectively, and both of them are proved NP-hard [48], even when $k = 2$.

Reduction: Considering graph G in Algorithm 1, choosing the optimal velocity profile of the charger equals finding the shortest path of G. In the multi-node scenario, n nodes equal k scenarios in MOSP and the value of the edge (i, j) can be represented as cost c_{ij}^n. Hence, MOSP can be reduced to finding the shortest path of G in the multi-node scenario.

Polynomial verification: Given n and k, we can uniquely build G and calculate the values of all edges in polynomial time $O(n^4)$[3].

4.2.2 Heuristic charging method

We first extend the velocity control method in Section 4.1.2 to the multi-node case and then prove the corresponding upper bound.

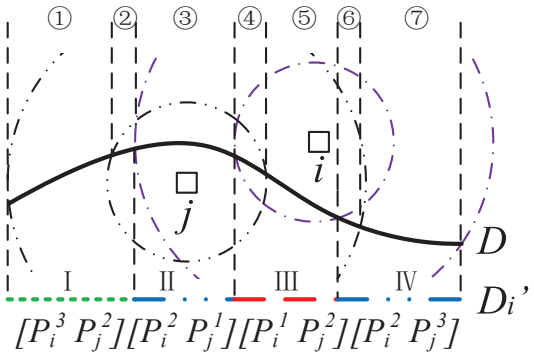

Figure 5. Trajectory discretization in multi-node charging scenario

With a given ϵ, we first draw concentric circles around each node to discretize the trajectory. Figure 5 shows an illustrative example. Trajectory D is divided into seven segments (① .. ⑦) by 4 concentric circles from node i and node j. As in the single node case, we replace the charging power at every position on the trajectory with the the charging power of different circles. In the multi-node case, the charging power on each circle at N nodes can be represented as an N-dimensional vector. Taking segment ① as an example, it has the charging power P_i^3 and P_j^2 with respect to node i and node j.

Due to the difficulty of joint optimization of charged energy among multiple nodes, we randomly choose one node as a "dominant node" after discretization and optimize its charged energy. Taking Figure 5 as an example, we choose node i as the dominant node. Therefore, instead of 7 segments divided by both node i and node j, we only focus on 4 segments divided by concentric circles of node i (Segments I to IV). For each segment divided by concentric circles of non-dominant nodes, we adopt the lower bound of the charging power of one segment as its approximate charging power vector. In Figure 5, we draw D_i' as the projection of D to show these four segments and their corresponding approximated charging power vectors. Taking Segment III as an example, it is not only located at the innermost zone of concentric circle of node i, but also bounded by the second smallest concentric circle of node j, and hence has the charging power vector $[P_i^1, P_j^2]$.

Once approximated charging power vectors of all segments are obtained, we can solve the velocity control problem in the multi-node charging scenario using Algorithm 1. We then shift

3. In our simulations, it leads to a reasonable running time (i.e., several minutes) on a commodity PC.

the dominant node and run the algorithm again until all N nodes have been visited. The best result among all N cases, achieving the maximal minimum charged energy, is used as the final result. Details of this algorithm are given below.

Algorithm 2 *Velocity Control Algorithm with Multiple Nodes*

```
Input: L, T, α, n, ϵ, p
Init minimum charged energy E* = 0
Discretize D based on ϵ and p
for each i ∈ [1, N] do
    Calculate the corresponding charging power vector
    Run Algorithm 1, get velocity profile R_i
    Given R_i, calculate charging energy E_{R_i} among all nodes
    if min E_{R_i} > E* then
        R* = R_i
    end if
end for
return R*
```

4.2.3 Performance Analysis

Let $E^i_{R^*_i}$ be the charged energy of node i under the *optimal velocity profile* R^*_i, i.e., the charged energy of the node which obtained the least amount of energy, and let $E_{R^*_i}(2)$ denote the charged energy of the node which has the second least amount of energy. Then, we have the following theorem.

Theorem 4.2. *$\max_i E_{R^*_i}(2)$ and $\min_i E^i_{R^*_i}$ are two upper bounds of the global optimal solution.*

Proof. Let $E^j_{R^*_k}$ denote the global optimal solution, the maximal minimum charging energy. That is, we can maximize the charged energy of the "bottleneck node" j under velocity profile R^*_k. Clearly, we have

$$E^j_{R^*_k} \leq E^q_{R^*_k}, q \neq j. \tag{15}$$

Since $\max_i E_{R^*_i}(1) \leq \max_i E_{R^*_i}(2)$, we have

$$E^j_{R^*_k} = E_{R^*_k}(1) \leq \max_i E_{R^*_i}(2), q \neq j \tag{16}$$

which proves $\max_i E_{R^*_i}(2)$ an upper bound of the global optimal solution. Moreover, since among all candidate velocity profiles $R^*_k, k \in [1, N]$, R^*_i is the optimal result with respect to node i, $E^i_{R^*_i}$ is the largest amount of energy node i can harvest. Assuming $\min_i E^i_{R^*_i} = E^q_{R^*_q}$, we have

$$\min_i E^i_{R^*_i} = E^q_{R^*_q} \geq E^q_{R^*_k}, k \neq q. \tag{17}$$

Combining (15) and (17), we have

$$\min_i E^i_{R^*_i} = E^q_{R^*_q} \geq E^q_{R^*_k} \geq E^j_{R^*_k}, k \neq q \tag{18}$$

which proves $\min_i E^i_{R^*_i}$, another upper bound of $E^j_{R^*_k}$. □

5 Special Case: Linear Trajectory

There exist numerous applications that require the charger to move on a straight line, including oil/gas/water pipeline monitoring [26], bridge and international border surveillance [27], coal mine tunnel underground monitoring [28], and unmanned vehicle monitoring in warehouse and inventory environments [13]). Unlike the 2D scenario covered in Section 4, for these applications we can solve the velocity control problem more efficiently, compute the optimal strategy for the single-node case, and then extend it to the multiple-node case.

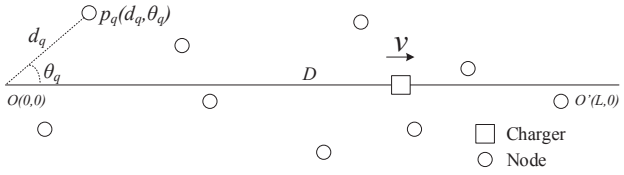

Figure 6. An example charging scenario with a linear moving trajectory

A typical charging scenario with a linear moving trajectory is shown in Figure 6. Without loss of generality, we assume trajectory D begins at the origin $O(0,0)$ and ends at $O'(L,0)$ (in a polar coordinate system). The position of each sensor node $p_q = (d_q, \theta_q)$, $\theta_q \neq 0$ and both initial and final velocities of the charger are 0. As a first step and to further clarify the problem, we analyze a simple charging scenario with a single node, and then extend it to the multi-node case in Section 5.2.

5.1 Single Node with a Linear Trajectory

As shown in Figure 7, in the single-node case, we need to maximize the charged energy of node q where $p_q = \{d_q, \theta_q\}$ given the patrolling cycle T of the charger. To this end, we first find the optimal velocity of the charger and then maximize the energy of the node at this specific velocity.

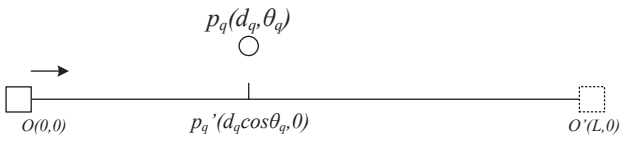

Figure 7. A single node charging with a linear trajectory

Before proposing the optimal velocity of the charger, we need the following two lemmas.

Lemma 5.1. *Node q achieves the maximal charged energy only if the acceleration of the charger $a_q(t) \in \{\alpha, -\alpha, 0\},\ t \in [0, T]$.*

Lemma 5.2. *Node q cannot achieve the maximal charged energy if the charger changes its acceleration more than twice before or after p'_q.*

Lemmas 5.1 and Lemma 5.2 jointly characterize the optimal velocity pattern of the charger during the entire patrolling cycle T. Specifically, Lemma 5.1 determines the optimal acceleration of the charger while Lemma 5.2 bounds the number of changes of acceleration of the charger. Both lemmas are proved by contradiction — we can always find a better velocity of the charger to increase the charged energy of the node if either of these lemmas is not satisfied. Detailed proofs of Lemmas 5.1 and 5.2 can be found in Section A and Section B respectively in the supplemental Appendix.

Based on these two Lemmas, we have the following corollary.

Corollary 5.3. *To achieve maximal charged energy on nodes, the velocity of the charger follows the blue curve in Figure 8 with slope (i.e., acceleration) $a \in \{\alpha, -\alpha\}$. In a special case when T is sufficiently large, the velocity pattern of the charger could be represented as the red dashed curve with $a \in \{\alpha, -\alpha, 0\}$.*

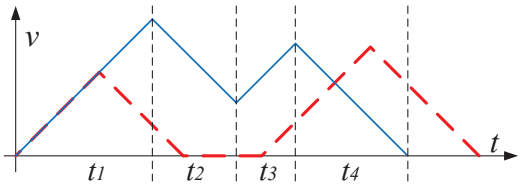

Figure 8. Optimal velocity pattern of the charger

Corollary 5.3 further defines two specific velocity patterns of the charger in the single node charging scenario. Mathematically, for the general case (the blue curve in Figure 8), we have

$$\begin{cases} t_1+t_2+t_3+t_4=T \\ t_1+t_3=t_2+t_4 \\ \frac{1}{2}t_1^2+t_1t_2-\frac{1}{2}t_2^2+(t_1-t_2)t_3+\frac{1}{2}t_3^2+\frac{1}{2}t_4^2=\frac{L}{a} \end{cases} \tag{19}$$

For the special case where T is sufficiently large (the red curve in Figure 8), we have $t_a = t_1 = t_2$, $t_b = t_3 = t_4$ and we call t_s as the *stop duration* of the charger. Therefore, we have

$$\begin{cases} t_a^2+t_b^2 & =\frac{L}{a} \\ 2t_a+t_s+2t_b & =T \end{cases} \tag{20}$$

Both (19) and (20) can be simplified and expressed by only two variables t_i and t_j. In other words, once t_i is fixed, we can calculate a unique set of t_j, $j \neq i$. Therefore, the total charged energy of the node can be represented solely by t_i. In order to obtain the optimal velocity profile of the charger, we only need to maximize charging energy function $E(t_i)$ (e.g., maximize $E(t_a)$). Detailed derivations of maximizing $E(t_i)$ can be found in Section C in the supplemental Appendix.

5.2 Multiple Nodes with a Linear Trajectory

In Section 5.1, we obtained the optimal velocity profile of the charger which maximizes the charged energy at node q. In multi-node case, based on the algorithm for the single node case, we successfully find an approximation solution.

5.2.1 Basic Idea

The basic idea is simple. First, we pick each of N nodes and calculate its corresponding optimal velocity profile $R_i, i \in [1, N]$ using the method proposed in Section 5.1. In the second step, for each node $j \neq i$, we calculate the charged energy $E_{R_i}(j)$ under each R_i. For instance, we first get the optimal velocity profile of the charger R_1 in the single node case with node 1, then calculate the charged energy of node 2 to node N sequentially with this specific velocity profile. In the last step, we use $R^* \in \{R_i\}, i \in [1, n]$ which maximizes the minimum charged energy among all nodes as the final result, i.e., $R^* = \max_i \min_j E_{R_i}(j)$.

5.2.2 Computation of Charged Energy

In the second step mentioned above, we need to calculate the charged energy at each node with a given R_i. It is non-trivial as energy integration with variable velocity is computationally expensive. So, we quantize the optimal velocity profile R_i which effectively reduces the computation complexity. Similar to Section 4.1.1, the minimal velocity increment/decrement is denoted as Δv and the time slot as Δt. In other words, $v(t+\Delta t) - v(t) = \{0, \Delta v, -\Delta v\}$. Therefore, considering the optimal velocity pattern of the charger as a discrete system, we have the following state-space equation.

$$\begin{bmatrix} v(k+1) \\ s(k+1) \end{bmatrix} = \begin{bmatrix} 1 & 0 \\ \Delta t & 1 \end{bmatrix} \begin{bmatrix} v(k) \\ s(k) \end{bmatrix} + \begin{bmatrix} \Delta v \\ 0 \end{bmatrix} f(k) \tag{21}$$

where $v(k)$ is the charger's velocity during time slot k, $s(k)$ is the cumulative traveling distance at the end of the k-th time slot and $f(k)$ represents the quantized optimal velocity profile where $f(k) = \{0, 1, -1\}$. The initial state of the system is $[v(0)\ s(0)]^T = [0\ 0]^T$.

Let E_{R_i} be the total charged energy at node i under R_i, then we can directly sum up the charged energy within each Δt to calculate E_{R_i}, i.e., $E_{R_i} = \sum E_i(k)$, where $E_i(k)$ is the charged energy at node i during time slot k. Given the optimal velocity profile, we know both $v(k)$ and $s(k)$. Hence, the charged energy during the k-th time slot can be expressed as

$$E_i(k) = \zeta \arctan \frac{2v(k)t + 2[s(k) - d_i \cos\theta_i]}{2d_i sin|\theta_i|}\Bigg|_0^{\Delta t}, \tag{22}$$

where $\zeta = \frac{\tau}{v(k)d_i sin|\theta_i|}$. Note that both of Δv and Δt can be small enough to make the quantization error negligible. The detailed derivation of (22) can be found in Section D in the supplemental Appendix.

5.2.3 Performance Analysis

Similar to the two-dimensional trajectory scenario, the optimal charging energy in the scenario with a linear trajectory is bounded by $\max_i E^1_{R_i}$ and $\min_i E^i_{R_i}$ as well. For a detailed explanation, see the proof of Theorem 4.2.

6 Evaluation

We now evaluate the performance of the proposed velocity control algorithms via extensive numerical simulations. We first present the simulation results for arbitrarily-shaped moving trajectories, followed by a single linear trajectory that represents many practical applications. We then illustrate the impact of system parameters, such as the number of nodes, energy-depletion rate and node distributions, on network performance. We use network lifetime and standard deviation of charged energy among the nodes in the network as the performance metrics in this evaluation. The network lifetime is represented by the energy balance of the node with minimum charged energy, and the standard deviation of charged energy among nodes represents charging fairness.

In our simulation, 50 wireless rechargeable sensor nodes are uniformly distributed in a 300m×300m area and the length of the linear trajectory is 300m. For the 2D trajectory, we randomly generate a non-crossing closed curve of the length of 1000m. Without loss of generality, we set $\tau = \frac{G_{tx}G_{rx}\eta}{L_p}(\frac{\lambda}{4\pi})^2 P_{tx} = 1$. In Section 6.1 and Section 6.2, energy-depletion rates of all nodes are set to 1 and we use charging energy and charged energy interchangeably. Results are averaged over 20 instances with different random seeds.

6.1 2D Irregular Trajectory

We present the results with different patrolling cycles T and maximum accelerations α for both single- and multi-node cases with a 2D irregular moving trajectory. We also compare the network performance of the proposed velocity control mechanism

with a baseline method in which the charger moves at a constant speed, i.e., $v(t) = L/T$. Note that the baseline method could perform better than our proposed method if the charger improperly spends too much time in areas with sparse node distribution.

6.1.1 Single-node case

The simulation results of the single-node case are plotted in Figure 9. We set the leftmost bar in each figure to 1 to normalize the charged energy of all nodes. Figure 9(a), as expected, shows that the charged energy of the node increases as the patrolling cycle T increases. For instance, given $\epsilon = 0.1$, the charged energy of a node has more than doubled when T is changed from 300 to 500. This could be explained by the fact that the charger spends more time charging the node when it is moving at a lower speed with a large patrolling cycle T. A similar trend can be found in Figure 9(b), where a higher maximum acceleration of the charger yields more charged energy at the node. However, the impact of incremental maximum acceleration on the charged energy is much less than that of the patrolling cycle. For example, when $\epsilon = 0.1$, the charged energy at the node for acceleration of the charger $9m/s^2$ is 4% higher than that for $5m/s^2$. In both Figures 9(a) and 9(b), we can see that a smaller ϵ brings more charging energy to the node. This is because the trajectory is divided into more segments with a smaller ϵ, providing chance for fine-grained velocity control. However, a larger ϵ incurs less computational overhead.

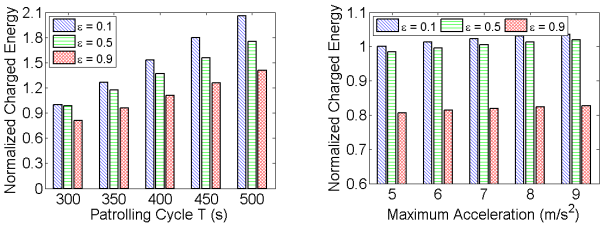

(a) Different patrolling cycles (b) Different α

Figure 9. Charged energy in the single-node charging scenario

Table 3
Comparison with the baseline method (single node case)

Patrolling Cycle	300	350	400	450	500
Baseline method	0.19	0.22	0.26	0.29	0.33
Proposed method	1.00	1.27	1.53	1.80	2.06

Table 3 compares the network lifetimes of the proposed velocity control algorithm and the baseline method. The network lifetime is shown to be extended significantly with the proposed velocity control. The average performance gap is as high as $6\times$ with different patrolling cycles.

6.1.2 Multi-node case

Figures 10(a) and 10(b) show how network lifetime improves as patrolling cycle T and maximum acceleration α increase. However, for a smaller patrolling cycle or maximum acceleration, the gain of the network lifetime for a small ϵ becomes less noticeable. For example, as illustrated in Figure 10(b), the lifetime gap between $\epsilon = 0.1$ and $\epsilon = 0.5$ decreases from 3.78 to 0.65 when the maximum acceleration of the charger decreases from $9m/s^2$ to $5m/s^2$. This is because the trajectory is divided into more segments with smaller ϵ, but the charger is unlikely to change its velocity in each segment due to its limited acceleration and the tight patrolling cycle requirement, thus making a limited improvement of the overall charging performance.

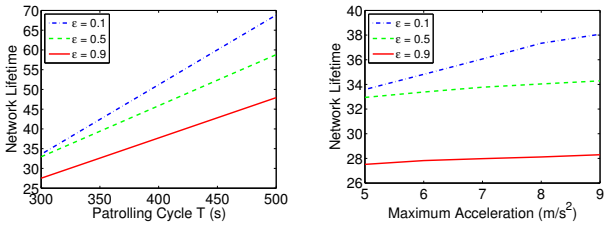

(a) Different patrolling cycles (b) Different α

Figure 10. Network lifetime in multi-node charging scenario

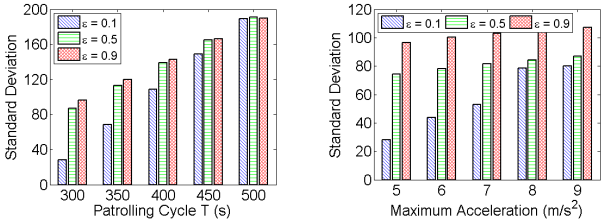

(a) Different patrolling cycles (b) Different α

Figure 11. Standard deviation of charged energy in the multi-node charging scenario

Figure 11 shows that the standard deviation of charged energy of nodes also increases with the growing patrolling cycle and maximum acceleration. This is due to the non-linear wireless charging model (1) and random distribution of sensor nodes. In other words, the growth rates of charged energy of nodes at different positions vary. Therefore, the more time the charger spends on charging, the larger energy gap will be between two nodes at different distances, increasing the standard deviation. Moreover, both Figures 11(a) and 11(b) show gaps of standard deviation between different values of ϵ to shrink with the growing patrolling cycle and maximum acceleration. For example, the gap between $\epsilon = 0.1$ and $\epsilon = 0.9$ decreases from 68.3 to 27.1 in Figure 11(b). This is not surprising since the segmentation of the trajectory plays a less prominent role if the charger has more time and higher acceleration capability.

Table 4
Comparison with baseline method (multi-node case)

Patrolling Cycle	300	350	400	450	500
Baseline method	16.5	19.3	22.1	24.8	27.6
Proposed method	33.6	42.4	51.2	60.0	68.9

Table 4 shows network lifetimes of the proposed and baseline velocity controls where the former always outperforms the latter. For example, when $T = 500$, the proposed velocity control mechanism extends network lifetime by $2.5\times$.

6.2 Linear Trajectory

We now present the simulation results with a linear trajectory. Since the optimal result can be obtained for the single node case with a linear trajectory, we only show the evaluation results of the multi-node case. To qualitatively analyze the velocity control performance, we also plot the analysis-based upper bound of the network lifetime.

Figures 12(a) and 12(b) show the network lifetime with the increasing patrolling cycles and maximum acceleration of the charger, respectively. Similar to the results of the 2D irregular trajectory, the network lifetime gradually increases with the growing maximum acceleration of the charger and the patrolling cycle. Moreover, the gap between our heuristic method and the upper-bound is relatively small and remains stable. Table 5 shows that the standard deviation of the charged energy of different nodes also increases with the increasing patrolling cycle. Due to the space limit, we omit the results of increasing maximum acceleration.

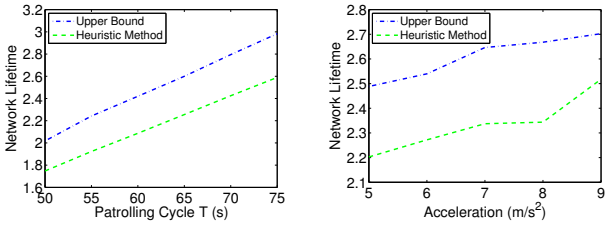

(a) Different patrolling cycles (b) Different α

Figure 12. Network lifetime with linear moving trajectory

Table 5
Standard deviations of charged energy of nodes

Patrolling Cycle	50	55	60	65	70	75
Standard Deviation	18.2	19.0	25.3	29.2	32.1	35.6

6.3 Impact of System Parameters

Let's examine how the number of sensors (i.e., node density) and node distribution affect the network performance.

6.3.1 Number of nodes

We compare the network lifetimes of linear and 2D moving trajectories while varying the number of nodes in the field. Figures 13(a) and 13(b) indicate a strong negative linear relation between the number of nodes and the network lifetime. For example, when the charger moves along a 2D irregular trajectory, the lifetime of the network with 20 nodes is 21.5% longer than that with 40 nodes, when $\epsilon = 0.1$ (62 vs. 51). This is because the network lifetime depends on the minimum charged energy among all nodes and the charger has limited time to fully charge all nodes in the network. Thus, there is more room for the velocity control algorithm with fewer nodes, allowing for more efficient charging of nodes. When the number of nodes increases, given the acceleration constraint and the patrolling cycle requirement, the charger needs to balance the charged energy among all nodes at different positions in order to maximize the network lifetime, thus degrading network lifetime. However, if the number of nodes keeps increasing, the network lifetime remains stable as the omnidirectional charging guarantees that most of nodes harvest more energy than the "bottleneck" node.

6.3.2 Heterogeneous energy depletion rate

In previous simulations, we assume an identical energy consumption rate of nodes, and therefore using homogeneous energy depletion rate. In this part, we consider heterogeneous energy depletion rate and examine its impact on charging performance. Since the power consumption pattern of nodes is influenced by a great many factors (e.g., applications, network topology, sensing/routing

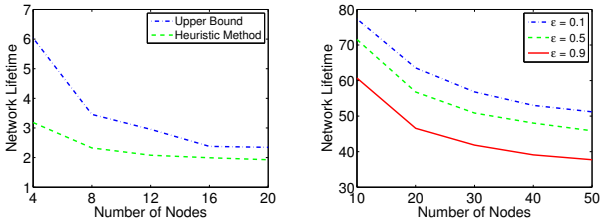

(a) With a linear trajectory (b) With a 2D trajectory

Figure 13. Impact of number of nodes

schedule etc.), here we simply use uniformly distributed random generated γ_i within the range of $[0.5, 1.5]$ to catch a glimpse of the impact of heterogeneous energy depletion rate.

Table 6
Network lifetime with different energy depletion rates

ϵ	0.1	0.3	0.5	0.7	0.9
Homogeneous γ_i	51.20	49.02	45.87	39.34	30.72
Heterogeneous γ_i	44.72	34.80	32.42	31.03	22.48

Table 6 shows the impact of the diverse energy depletion rates. Compared with homogeneous network, network lifetime degrades with diverse γ_i. This is because the charger has to spend more time taking care of the larger quantity of energy-hungry nodes exist in the heterogeneous network, therefore impairing the charged energy on other nodes.

6.3.3 Varying node distribution

So far, we assumed sensor nodes to be uniformly distributed. We now evaluate the performance of the proposed velocity control algorithms under normal and gamma distributions of sensors and compare them with the results of uniform distribution. In the case of normal distribution, we generate positions of nodes with mean position at the center of the area and variance $\sigma = 50$ while in the case of gamma distribution, we set the shape parameter $k = 1$ and the scale parameter $\theta = 2$. To avoid bias caused by different shapes of 2D trajectories, we only focus on the linear trajectory in this part of evaluation. Examples of three different distributions are shown in Figures 14(a), 14(b) and 14(c), respectively.

Figures 14(d), 14(e) and 14(f) show network lifetime, average charged energy and standard deviation of charged energy of different nodes, respectively. Figures 14(d) and 14(e) show that both network lifetime and average charged energy of normal distribution are superior to those of other two distributions, because in normal distribution where nodes are close to each other, the charged energy of the remote nodes is higher than that of remote nodes in uniform and gamma distributions. Moreover, since the charger can spend most of time charging the central area where the majority of nodes are located, the average charged energy of nodes is maximized in the normal distribution scenario. On the contrary, in the gamma distribution, a large portion of nodes are located near the edge of the sensing area, thus decreasing the average charged energy.

In Figure 14(f), unsurprisingly, the standard deviation of charged energy under the gamma distribution is found much smaller than that of the other two distributions, because the majority of nodes in case of gamma distribution are located far away from the moving trajectory. Although charged energy varies, the relatively low charged energy of nodes yields a small standard

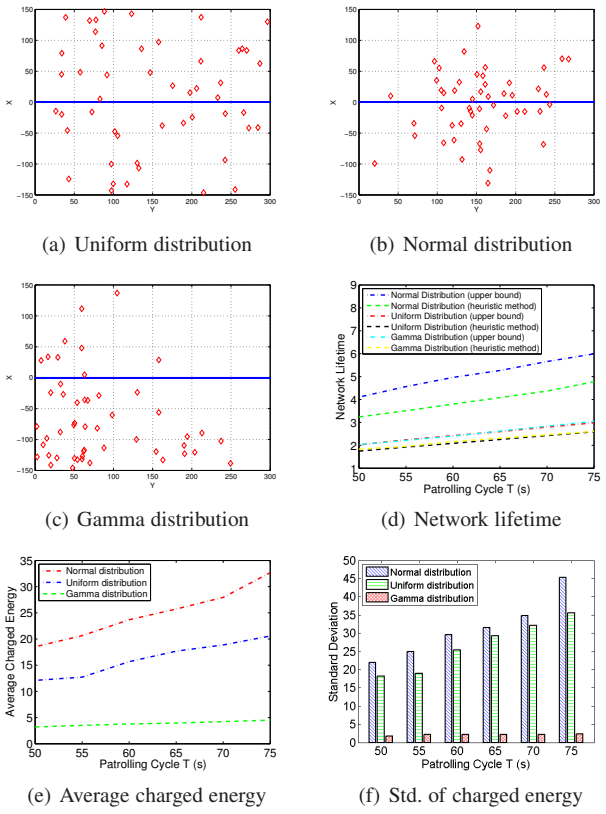

(a) Uniform distribution (b) Normal distribution

(c) Gamma distribution (d) Network lifetime

(e) Average charged energy (f) Std. of charged energy

Figure 14. Different node distributions with a linear trajectory

deviation. However, in normal and uniform distributions, where the average charged energy are much greater, variations of the large amount of charged energy result in large standard deviations.

7 Discussion

7.1 Impact of initial energy of nodes

In this paper, we proposed how to maximize the charged energy of nodes in the network. However, our design is adaptive to a more general scenario that accounts for initial energy of nodes. In such a case, we aim to maximize the total energy of nodes after each patrolling cycle of the charger. In the special case with a linear trajectory, we only need to add the initial energy of nodes during the process of charged energy computation (Section 5.2.2). For the charging scenario with a 2D irregular trajectory, we can add the initial energy balance of each node during the initialization of optimal substructure. Specifically, we add the initial energy balance of each node to $A(n, 1)$ in Figure 4 when running Algorithm 1.

7.2 On Network Lifetime

In this paper, we focused on maximizing the charged energy of the node which has the least amount of energy (a.k.a. the "bottleneck node") among all nodes in order to maximize network lifetime of a WRSN. However, the charged energy of other nodes may suffer in this charging scenario. For example, if there is a node far from the moving trajectory, the charger needs to spend plenty of time trying to charge this node, thus reducing the overall charged energy for all nodes. Therefore, one question may be: "if energy depletion of some nodes is allowed (e.g., in a dense WSN), which part of nodes shall we sacrifice to maximize the charging performance of the remaining part of the network?" In other words, we want to know how much better we can charge if we consider fewer nodes in the network.

Consider the charging scenario with a 2D trajectory as an example. We first run Algorithm 2 once, and find the "bottleneck node" i, the node which could be least charged even under the optimal velocity pattern of the charger. We then exclude node i and run the algorithm again to find a new "bottleneck" j. We repeat this process and rank all nodes based on their capability of being charged. This way, we can quantitatively determine the impact of each node on the charging performance of the entire WSN and maximize the lifetime of the node with the M-th minimum charged energy in the network. For example, we can calculate the improvement of overall charging energy without considering x nodes with the least "capability of being charged".

7.3 Dissimilar Acceleration and Deceleration Bound

In Section 3.2, we consider a unique bound for acceleration and deceleration. However, both of our algorithms in 1D and 2D scenarios are compatible with separate acceleration and deceleration bounds. Specifically, let α_{acc} and α_{dec} be the bounds of acceleration and deceleration respectively. For the 2D case, we have to rewrite (6) as

$$\begin{cases} |v_i - v_{i-1}| \leq \alpha_{acc} t_i, & v_i - v_{i-1} \geq 0 \\ |v_i - v_{i-1}| \leq \alpha_{dec} t_i, & v_i - v_{i-1} < 0 \end{cases} \tag{23}$$

and revise (10) as well as the connection rule accordingly. For the special case with a linear trajectory, we replace the previous deceleration bound $-\alpha$ with α_{dec} and prove Lemmas 5.1, Lemma 5.2 and Corollary 5.3 using the same methodology.

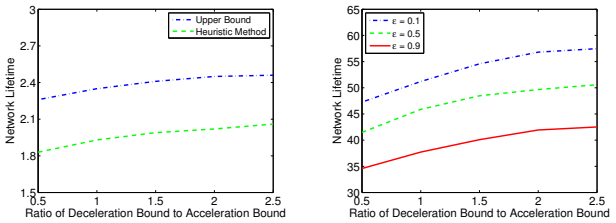

(a) With a linear trajectory (N=20) (b) With a 2D trajectory (N=50)

Figure 15. Dissimilar Acceleration and Deceleration Bound

Figure 15 shows the network lifetime with separate bounds of acceleration and deceleration. We set $\alpha_{acc} = 1$ and the x-axis in Figure 15 is the ratio of the deceleration bound to the acceleration bound. Similar to Figure 10(b), in this figure, network lifetime increases with a growing ratio (i.e., large deceleration bound). For example, in the 2D scenario, the average extension of network lifetime is 10.14% when the deceleration bound changes from 1 to 2. It is because with a better deceleration capability, the charger is able to broadcast energy at places close to nodes for a longer period of time.

8 Conclusion

In this paper, we studied the problem of maximizing network lifetime in a general scenario, where a charger travels through a predefined arbitrarily-shaped trajectory and charges the randomly deployed sensor nodes in a WRSN. We formulated the main problem as a charger velocity control problem subject to the constraints of patrolling cycle and acceleration limit. A novel

spatial-temporal discretization method was used for this NP-hard problem and a suboptimal solution was proposed with some provable performance bounds. We then simplified the charging path to a linear trajectory that represents many real wireless charging applications and derived the optimal results. Finally, we conducted extensive simulations to evaluate the performance of the proposed algorithms. The results demonstrated that the proposed velocity control mechanism achieves $2.5\times$ network lifetime extension compared to the baseline method. As part of our future research direction, we are extending the charging model to non-omnidirectional one. In addition, joint optimization of moving trajectory and velocity is also worth investigating.

ACKNOWLEDGMENTS

This work was partially supported by 973 Program under grant 2015CB352503, NSFC under grant 61228302, ZJSF under grant LY14F030016 and scholarship funded by China Scholarship Council. Jiming Chen is the corresponding author of this paper.

REFERENCES

[1] S. He, J. Chen, F. Jiang, D.K.Y. Yau, G. Xing, and Y. Sun. Energy provisioning in wireless rechargeable sensor networks. *IEEE Transactions on Mobile Computing*, 12(10):1931–1942, Oct 2013.

[2] Jiming Chen, Junkun Li, and T.H. Lai. Energy-efficient intrusion detection with a barrier of probabilistic sensors: Global and local. *IEEE Trans. on Wireless Commun.*, 12(9):4742–4755, September 2013.

[3] Jiming Chen, Junkun Li, Shibo He, Tian He, Yu Gu, and Youxian Sun. On energy-efficient trap coverage in wireless sensor networks. *ACM Trans. Sen. Netw.*, 10(1):2:1–2:29, December 2013.

[4] H. Yousefi, M. H. Yeganeh, N. Alinaghipour, and A. Movaghar. Structure-free real-time data aggregation in wireless sensor networks. *Computer Communications*, 35(9):1132–1140, 2012.

[5] H. Yousefi, M. Malekimajd, M. Ashouri, and A. Movaghar. Fast aggregation scheduling in wireless sensor networks. *IEEE Transactions on Wireless Communications*, 14(6):3402–3414, 2015.

[6] WPC. Magnetic Resonance and Induction. http://goo.gl/J0ifVk.

[7] Qi. The Wireless Power Consortium. http://goo.gl/BTuTb.

[8] Powercast Inc. Powercast Debuts RF Energy Harvesting Kit for Wireless Battery Charging. http://goo.gl/JRLNBy.

[9] A. P. Sample, D. J. Yeager, P. S. Powledge, A. V. Mamishev, and J. R. Smith. Design of an RFID-based battery-free programmable sensing platform. *IEEE Trans. Instrum. Meas.*, 57(11):2608–2615, 2008.

[10] Sensor Systems Laboratory. WARP (Wireless Ambient Radio Power). http://sensor.cs.washington.edu/WARP.html.

[11] rezence.com. A4WP and PMA Merger Announcement. https://www.rezence.com/alliance/a4wp-pma-merger.

[12] D. J.A. Bijwaard, W. A.P. van Kleunen, P. J.M. Havinga, L. Kleiboer, and M. J.J. Bijl. Industry: using dynamic WSNs in smart logistics for fruits and pharmacy. In *ACM SenSys*, 2011.

[13] G. Liu, W. Yu, and Y. Liu. Resource management with RFID technology in automatic warehouse system. In *IEEE IROS*, 2006.

[14] M. Buettner, R. Prasad, M. Philipose, and D. Wetherall. Recognizing daily activities with RFID-based sensors. In *ACM Ubicomp*, 2009.

[15] Yuanchao Shu, Yu (Jason) Gu, and Jiming Chen. Dynamic authentication with sensory information for the access control systems. *IEEE Transactions on Parallel and Distributed Systems*, 25(2):427–436, 2014.

[16] M. D. Todd G. Park D. Mascarenas, E. Flynn and C. R. Farrar. Wireless sensor technologies for monitoring civil structures. *Sound and Vibration*, 42(4):16–21, 2008.

[17] S. Zhang, J. Wu, and S. Lu. Collaborative mobile charging for sensor networks. In *IEEE MASS*, 2012.

[18] L. Xie, Y. Shi, Y. T. Hou, W. Lou, and H. D. Sherali. On traveling path and related problems for a mobile station in a rechargeable sensor network. In *ACM MobiHoc*, 2013.

[19] L. Fu, P. Cheng, Y. Gu, J. Chen, and T. He. Minimizing charging delay in wireless rechargeable sensor networks. In *IEEE INFOCOM*, 2013.

[20] P. Kellett. Robotic warehousing: a new market opportunity for robot manufacturers and integrators? http://goo.gl/h0kwAU.

[21] W. Alsalih, H. Hassanein, and S. Akl. Routing to a mobile data collector on a predefined trajectory. In *IEEE ICC*, 2009.

[22] M. Zhao, J. Li, and Y. Yang. A framework of joint mobile energy replenishment and data gathering in wireless rechargeable sensor networks. *IEEE Trans. on Mobile Comput.*, 13(12):2689–2705, Dec 2014.

[23] S. Guo, C. Wang, and Y. Yang. Mobile data gathering with wireless energy replenishment in rechargeable sensor networks. In *IEEE INFOCOM*, 2013.

[24] L. Xie, Y. Shi, Y. T. Hou, W. Lou, H. D. Sherali, and S. F. Midkiff. Bundling mobile base station and wireless energy transfer: modeling and optimization. In *IEEE INFOCOM*, 2013.

[25] E. Melachrinoudis C. Petrioli S. Basagni, A. Carosi and Z. M. Wang. Controlled sink mobility for prolonging wireless sensor networks lifetime. *Wireless Networks*, 14:831–858, 2008.

[26] I. Jawhar and N. Mohamed. A hierarchical and topological classification of linear sensor networks. In *WTS*, 2009.

[27] A. D'Costa, V. Ramachandran, and A. M. Sayeed. Distributed classification of gaussian space-time sources in wireless sensor networks. *IEEE J. Sel. Areas Commun.*, 22(6):1026–1036, Aug 2004.

[28] X. Xu, J. Luo, and Q. Zhang. Delay tolerant event collection in sensor networks with mobile sink. In *IEEE INFOCOM*, 2010.

[29] A. Kurs, A. Karalis, R. Moffatt, J. D. Joannopoulos, P. Fisher, and M. Soljacic. Wireless power transfer via strongly coupled magnetic resonances. *Science*, 317:83–86, 2007.

[30] Yuanchao Shu, Peng Cheng, Yu Gu, Jiming Chen, and Tian He. Minimizing communication delay in RFID-based wireless rechargeable sensor networks. In *IEEE SECON*, 2014.

[31] Y. Peng, Z. Li, W. Zhang, and D. Qiao. Prolonging sensor network lifetime through wireless charging. In *IEEE RTSS*, 2010.

[32] Y. Shi, L. Xie, Y. T. Hou, and H. D. Sherali. On renewable sensor networks with wireless energy transfer. In *IEEE INFOCOM*, 2011.

[33] Liguang Xie, Yi Shi, Y. Thomas Hou, Wenjing Lou, Hanif D. Sherali, and Scott F. Midkiff. On renewable sensor networks with wireless energy transfer: The multi-node case. In *IEEE SECON*, 2012.

[34] Liguang Xie, Yi Shi, Y.T. Hou, Wenjing Lou, H.D. Sherali, and S.F. Midkiff. Multi-node wireless energy charging in sensor networks. *IEEE/ACM Transactions on Networking*, 23(2):437–450, April 2015.

[35] K. Li, H. Luan, and C. C. Shen. Qi-ferry: energy-constrained wireless charging in wireless sensor networks. In *IEEE WCNC*, 2012.

[36] Constantinos Marios Angelopoulos, Sotiris Nikoletseas, and Theofanis P. Raptis. Wireless energy transfer in sensor networks with adaptive, limited knowledge protocols. *Computer Networks*, 70:113–141, September 2014.

[37] H. Dai, L. Xu, X. Wu, C. Dong, and G. Chen. Impact of mobility on energy provisioning in wireless rechargeable sensor networks. In *IEEE WCNC*, 2013.

[38] P. Cheng, S. He, F. Jiang, Y. Gu, and J. Chen. Optimal scheduling for quality of monitoring in wireless rechargeable sensor networks. *IEEE Transactions on Wireless Communications*, 12(6):3072–3084, 2013.

[39] Cong Wang, Ji Li, Fan Ye, and Yuanyuan Yang. Multi-vehicle coordination for wireless energy replenishment in sensor networks. In *IEEE IPDPS*, 2013.

[40] Haipeng Dai, Xiaobing Wu, Guihai Chen, Lijie Xu, and Shan Lin. Minimizing the number of mobile chargers for large-scale wireless rechargeable sensor networks. *Computer Commun.*, 46:54–65, 2014.

[41] Adelina Madhja, Sotiris Nikoletseas, and Theofanis P. Raptis. Efficient, distributed coordination of multiple mobile chargers in sensor networks. In *ACM MSWiM*, pages 101–108, 2013.

[42] Z. Li, Y. Peng, W. Zhang, and D. Qiao. J-RoC: a joint routing and charging scheme to prolong sensor network lifetime. In *IEEE ICNP*, 2011.

[43] Songtao Guo, Cong Wang, and Yuanyuan Yang. Joint mobile data gathering and energy provisioning in wireless rechargeable sensor networks. *IEEE Trans. on Mobile Comput.*, 13(12):2836–2852, Dec 2014.

[44] Yuanchao Shu, Peng Cheng, Yu Gu, Jiming Chen, and Tian He. TOC: Localizing Wireless Rechargeable Sensors with Time of Charge. *ACM Trans. Sen. Netw.*, 11(3):44:1–44:22, February 2015.

[45] Liang He, Peng Cheng, Yu Gu, Jianping Pan, Ting Zhu, and Cong Liu. Mobile-to-mobile energy replenishment in mission-critical robotic sensor networks. In *IEEE INFOCOM*, 2014.

[46] G. Tsaggouris and C. D. Zaroliagis. Multiobjective optimization: improved FPTAS for shortest paths and non-linear objectives with applications. *Theory Comput. Syst.*, 45(1):162–186, 2009.

[47] H. Aissi, C. Bazgan, and D. Vanderpooten. General approximation schemes for min-max (regret) versions of some (pseudo-)polynomial problems. *Discrete Optimization*, 7(3):136–148, 2010.

[48] X. Gandibleux, F. Beugnies, and S. Randriamasy. Martins' algorithm revisited for multi-objective shortest path problems with a MaxMin cost function. *4OR*, 4(1):47–59, 2006.

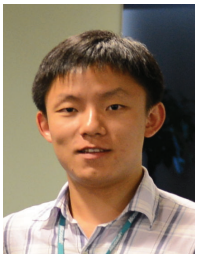

Yuanchao Shu (IEEE S'12-M'15) received the Ph.D. degree from Zhejiang University in 2015. He is currently an Associate Researcher at Microsoft Research Asia. From 2013 to 2015, he was a joint Ph.D. student in Computer Science at University of Michigan, Ann Arbor. He is the author and co-author of over 10 papers in premier journals and conferences, including IEEE JSAC, IEEE TMC, IEEE TPDS, ACM MobiCom, IEEE INFOCOM, and is the recipient of the IBM PhD Fellowship and the INFOCOM'14 Best Demo Award. His research interests include cyber-physical systems, mobile computing, wireless sensor network and big data analysis. He is a member of ACM and IEEE.

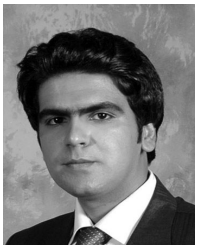

Hamed Yousefi is currently a Ph.D. candidate of computer engineering at Sharif University of Technology in Tehran, Iran where he received his M.Sc. in 2009. From 2013 to 2014, he was a visiting Ph.D. student at the department of computer science, University of Michigan, Ann Arbor, USA. He is a member of Iranian Inventors Association. His research interests include wireless networks, performance and dependability modeling, and real-time communications.

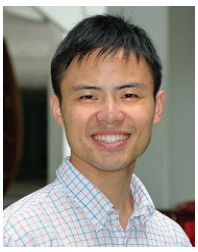

Peng Cheng (IEEE M'10) received the B.E. degree in Automation, and the Ph.D. degree in Control Science and Engineering in 2004 and 2009 respectively, both from Zhejiang University, Hangzhou, P.R. China. Currently he is Associate Professor with the Department of Control Science and Engineering, Zhejiang University. He serves as Associate Editor for Wireless Networks, International Journal of Communication systems, and Guest Editor for IEEE Transactions on Control of Network Systems. He serves/served as Local Arrangement Chair for IEEE MobiHoc 2015, and Publicity co-Chair for IEEE MASS 2013. His research interests include networked sensing and control, cyber-physical systems, robust control and applications.

Jiming Chen (IEEE M'08-S'M'11) received B.Sc degree and Ph.D degree both in Control Science and Engineering from Zhejiang University in 2000 and 2005, respectively. He was a visiting researcher at INRIA in 2006, National University of Singapore in 2007, and University of Waterloo from 2008 to 2010. Currently, he is a full professor with Department of control science and engineering, and vice director of the State Key laboratory of Industrial Control Technology and Institute of Industrial Process Control at Zhejiang University, China. He currently serves associate editors for several international Journals including IEEE Transactions on Parallel and Distributed System, IEEE Network, IEEE Transactions on Control of Network Systems, *etc.* He was a guest editor of IEEE Transactions on Automatic Control,etc. His research interests include sensor networks, networked control.

Yu (Jason) Gu is currently a Research Staff Member at IBM Watson Health. He received the Ph.D. degree from the University of Minnesota, Twin Cities in 2010. Dr. Gu is the author and co-author of over 100 papers in premier journals and conferences. His publications have been selected as graduate-level course materials by over 20 universities in the United States and other countries. His research includes Networked Embedded Systems, Wireless Sensor Networks, Cyber-Physical Systems, Wireless Networking, Real-time and Embedded Systems, Distributed Systems, Vehicular Ad-Hoc Networks and Stream Computing Systems. Dr. Gu is a member of ACM and IEEE.

Tian He is currently an Associate Professor in the Department of Computer Science and Engineering at the University of Minnesota-Twin City. He received the Ph.D. degree under Professor John A. Stankovic from the University of Virginia, Virginia in 2004. Dr. He is the author and co-author of over 190 papers in premier network journals and conferences with over 15,000 citations (H-Index 48). His publications have been selected as graduate-level course materials by over 50 universities in the United States and other countries. Dr. He has received a number of research awards in the area of networking, including five best paper awards. Dr. He is also the recipient of the NSF CAREER Award 2009 and McKnight Land-Grant Professorship. Dr. He served a few program chair positions in international conferences and on many program committees, and also currently serves as an editorial board member for six international journals. His research includes wireless sensor networks, cyber-physical systems, intelligent transportation systems, real-time embedded systems and distributed systems, supported by NSF, IBM, Microsoft and other agencies.

Kang G. Shin (IEEE L'F'12) is currently the Kevin and Nancy OConnor Professor of Computer Science with the Department of Electrical Engineering and Computer Science, University of Michigan, Ann Arbor, MI, USA. He has been a Cofounder of a couple of start-ups and has also licensed some of his technologies to industry. He has supervised the completion of 74 Ph.D. studies. He has authored/coauthored over 800 technical articles (more than 300 of these are in archival journals), a textbook, and over 20 patents or invention disclosures. His current research focuses on QoS-sensitive computing and networking and on embedded real-time and cyber-physical systems.

Prof. Shin received numerous best paper awards, including the Best Paper Awards from the 2011 ACM International Conference on Mobile Computing and Networking (MobiCom11), the 2011 IEEE International Conference on Autonomic Computing, and the 2010 and 2000 USENIX Annual Technical Conferences, the 2003 IEEE Communications Society William R. Bennett Prize Paper Award, and the 1987 Outstanding IEEE Transactions on Automatic Control Paper Award. He has also received several institutional awards, including the Research Excellence Award in 1989, the Outstanding Achievement Award in 1999, the Distinguished Faculty Achievement Award in 2001, and the Stephen Attwood Award in 2004 from the University of Michigan (the highest honor bestowed to Michigan Engineering faculty); a Distinguished Alumni Award of the College of Engineering, Seoul National University in 2002; the 2003 IEEE RTC Technical Achievement Award; and the 2006 Ho-Am Prize in Engineering (the highest honor bestowed to Korean-origin engineers).